Directional light scanning laser ophthalmoscope

Brian Vohnsen, Ignacio Iglesias, and Pablo Artal

Laboratorio de Óptica, Universidad de Murcia, Campus de Espinardo (Edificio C), 30071 Murcia, Spain

Received March 4, 2005; revised manuscript received May 10, 2005; accepted May 16, 2005

The cone photoreceptor mosaic of the living human eye has in a limited number of cases been imaged without the use of wavefront-correction techniques. To accomplish this, the directionality of the photoreceptors, as manifested by their waveguiding properties, may be used to advantage. In the present paper we provide a model of our recently proposed directional light scanning laser ophthalmoscope [Opt. Lett. **29**, 968 (2004)] together with a detailed numerical analysis of the device. The outcome is compared with experimental results.

OCIS codes: 170.4470, 170.5810, 330.5310.

1. INTRODUCTION

The optical performance of the normal human eye deteriorates at large pupil diameters owing to the presence of aberrations. Aberrations also limit the resolution that can be attained with ocular imaging devices. Thus, to get beyond this limitation the aberrations need to be compensated for. The introduction of adaptive optics in studies of the eye[1–4] has allowed for correction of even higher-order aberrations in essentially real time and thereby has led to the acquisition of high-resolution retinal images. Nevertheless, these results are somewhat contradicted by reported cone photoreceptor mosaic images obtained in the living eye without the aid of wavefront-correction methods.[5–7]

The Stiles–Crawford effect refers to the reduced visual sensitivity to light that is incident off the pupil center and therefore obliquely incident on the retina.[8,9] A similar phenomenon occurs for light reflected off the retina[10–13] where it is typically known as the optical Stiles–Crawford effect. Based on this observation, we recently introduced a confocal scanning laser ophthalmoscope (c-SLO) designed to make use of the directionality of reflected light in high-resolution retinal imaging.[7] This technique relies on an accurate alignment of the incident beam (chosen sufficiently narrow to reduce the influence of aberrations) at the pupil point where its visibility is maximized, i.e., at the peak of the Stiles–Crawford effect. In this way the coupling of light at the retina to the underlying photoreceptors is maximized (allowing for the largest signal).[10,14] At the confocal detection a sufficiently small pinhole is chosen to highlight the contribution of directional backreflected light produced by the waveguiding of the photoreceptors.[7] The photoreceptors permit waveguiding with negligible absorption if bleached or if near-IR illumination is used, and a major fraction of the returning light can therefore be directional.[11,15]

Generally, this light has suffered less from aberrations than broadly scattered light since it exits the eye mostly through a fraction of the entire pupil area.[11] A valid alternative would be a reduced exit pupil at the eye although this would presumably require additional transverse alignment to be properly centered at the peak of the (optical) Stiles–Crawford effect (which is often displaced from the apparent pupil center).[8,12,13] The use of a small confocal pinhole has the additional advantage of highlighting the contribution of scattering sources (both guided and nonguided light) located in the plane of the retina conjugate to the pinhole while discriminating against scattered light from elsewhere that could deteriorate image quality.

In this paper we make a numerical analysis of the imaging capabilities of the technique in order to gain further insight and, in particular, to examine under what circumstances the c-SLO may be used to directly access parameters of the photoreceptor mosaic even in the absence of wavefront correction. The model will be used on light that originates in photoreceptor waveguiding (as from bleached or nonabsorbing cones), but it should be stressed that the same approach can easily be generalized to handle imaging of arbitrary scattering sources (not only photoreceptor waveguides) by a simple modification of their pupil field. The paper is organized as follows. In Section 2 a model of the directional light c-SLO is described. Section 3 contains a numerical analysis in which the importance of various physical parameters (pinhole size, photoreceptor diameter, etc.) is studied in order to elucidate their influence on high-resolution retinal images, and the outcome is compared with experimental results. In Section 4 we present our conclusions.

2. MODEL OF THE DIRECTIONAL LIGHT SCANNING LASER OPHTHALMOSCOPE

In this section the model constructed to analyze our recently proposed directional light c-SLO is discussed.[7] The description includes only directional light produced by cone photoreceptor waveguiding; consequently scattering from all other retinal structures has been omitted. This assumption is justified by the often large contribution of directional light compared with broadly scattered light[11,15] and by the selectivity of the confocal pinhole.[7]

On the basis of a simulation of the optical Stiles–Crawford effect, and in agreement with the findings of others,[16] we have recently found that the light reflected

from each cone photoreceptor may be dominated by the fundamental waveguide mode of each inner segment.[14] This mode can be well approximated by a Gaussian function of the type $\exp(-r^2/w_m^2)$, where r is the radial distance from the photoreceptor axis and w_m is the half-width of the mode (which is related to the diameter of the inner segment). Thus, in the following we assume that each illuminated photoreceptor radiates a Gaussian beam of light directed toward the center of the pupil[17] as shown schematically in Fig. 1. It may be noted that the intensity distribution produced at the pupil for a single photoreceptor is Gaussian, too, in agreement with the commonly used model for the (optical) Stiles–Crawford effect when a directionality parameter is sought.[14] A shift away from the pupil center can easily be incorporated by translating the Gaussian distribution in the pupil plane.

For simplicity, the incident beam scanning of the c-SLO is omitted at first. Instead, an image is considered to be formed by scanning with the confocal pinhole across a steady image plane (where all contributing photoreceptors are brought to a focus) while recording the transmitted light power versus position. Leaving out the incident beam scanning simplifies the analysis of the imaging process and corresponds to the realistic case of a poorly focused beam that simultaneously illuminates several photoreceptors. Nevertheless, it should be kept in mind that the dual scanning of an actual confocal system can lead to improved image resolution and contrast.[18]

Wavefront aberrations too will have a detrimental effect on the quality of recorded images but may be reduced by either customized phase plates[19] or adaptive optics.[1,2,4,20] The wavefront aberrations $\mathbf{\Phi}_{\mathrm{WA}}$ of the real eye and system, as measured with a Hartmann–Shack sensor in a plane conjugate to the eye pupil,[21] can be included in the model by introducing them on each Gaussian beam. It may be assumed that each beam suffers identical aberrations (apart from the tilt that separates them) when scanning only a small retinal area. A similar situation arises in experiments with wavefront correction where an average is used during the rapid image acquisition.[1,2,4,20]

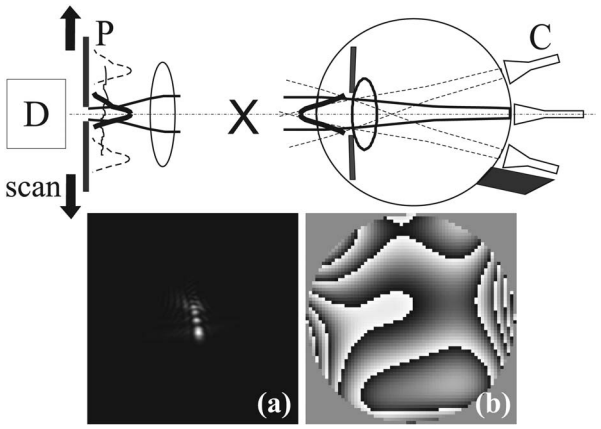

Fig. 1. Schematic of the model used to describe c-SLO imaging with directional light detection including Gaussian beam radiation from each cone photoreceptor (C), confocal pinhole (P), and detector (D). Also shown is (a) point-spread function calculated from the (b) measured wavefront aberration of an eye shown on a 2π phase map (6.0 mm pupil at a wavelength of 0.785 μm). The aberration, although dominated by astigmatism, includes up to 4th-order Zernike polynomials with a total RMS value of $\sim$0.67 μm.

Thus, the field in the plane of the confocal pinhole from N simultaneously illuminated photoreceptors can be expressed via the Fourier transform of the (scaled) pupil field as

$$\mathcal{F}\{\psi_{\mathrm{pupil}}\} = \sum_{j=1}^{N} \mathcal{F}\left\{ A \exp\left[i\mathbf{\Phi}_{\mathrm{WA}}(x,y) - \frac{x^2+y^2}{w_p^2} \right] \right\} \otimes \boldsymbol{\delta}(\mathbf{r}-\mathbf{r}_j), \tag{1}$$

where $\otimes$ denotes a convolution. In this expression w_p is the spot size at the pupil of the reflected Gaussian beam which at wavelength λ is related to the photoreceptor mode through $w_p = \lambda f_{\mathrm{eye}}/\pi n_{\mathrm{eye}} w_m$ [i.e., the standard relation between pupil field width and focal spot size (here the waveguide mode) for a Gaussian beam in a homogenous medium]. Here $f_{\mathrm{eye}} = 22.2$ mm and $n_{\mathrm{eye}} = 1.33$ in the reduced eye model. In Eq. (1) the unaberrated image of the jth photoreceptor is centered at $\mathbf{r}_j$ in the pinhole plane, and the Fourier transform is carried out at frequencies that take into account the system magnification as well as the focal length of the lens nearest the pinhole. Although it has been written explicitly for Gaussian beams, the equation may also be used to simulate imaging of retinal structures other than photoreceptor waveguides by simply replacing the Gaussian amplitude weighting with a different pupil field (a uniform pupil would be representative, e.g., of a pointlike scattering object located in the retinal plane, and out-of-focus features can be considered through their phase variation at the pupil). Thus, with only small modifications the model would be suitable to analyze imaging of retinal structures other than photoreceptor waveguides.

In the present situation, the best possible cone mosaic image will show an extended bright spot (corresponding to the mode width) at the location of each imaged photoreceptor. This differs somewhat from the common situation in confocal microscopy where a point object is imaged as a spot because of the finite size of the numerical aperture (here the waveguide objects have a finite width). For convenience of modeling, it has been assumed that all contributing photoreceptors radiate with equal power and phase as contained in the amplitude factor A. This simplification can easily be undone by inclusion of a complex field scaling factor at each $\mathbf{r}_j$ to take into account, e.g., differences in the phase of beams radiated by neighboring photoreceptors.[14,22] It should be mentioned, though, that if the exposed retinal area is very small, as in a c-SLO, the simultaneously illuminated photoreceptors are highly similar,[23] and differences in phase of the reradiated light are therefore expected to be small. In contrast, for an extended retinal area, with numerous photoreceptors exposed to light in unison (as in fundus photography), this is presumably no longer the case and the phase may play a more important role.[14,22]

The image $I(\mathbf{r})$ obtained by scanning with the confocal pinhole $\mathcal{P}(\mathbf{r})$ can (apart from a scaling constant) be expressed as

$$I(\mathbf{r}) = |\mathcal{F}\{\psi_{\text{pupil}}\}|^2 \otimes \mathcal{P}(\mathbf{r}). \quad (2)$$

Although we have assumed that all photoreceptors return an identical amount of light this can be expected to vary in a real experiment. This may result in an inhomogeneous distribution of brightness that in the presence of noise can make the photoreceptor density seem lower than it actually is. This can occur if the photoreceptor reflectivity changes (spatially or temporally), or if the coupling efficiency varies as a result of nonuniform illumination, photoreceptor tilt, or the scanning in itself. Variations should also be expected when different sized photoreceptors are scanned. Actually, time-dependent variations in the amount of reflected light from individual photoreceptors have been reported on a long time scale,[15] but this factor has hardly a measurable influence during the rapid acquisition of a single c-SLO image. Reflectivity changes, however, may influence subsequently recorded frames (in our present experimental system the frame rate is 15 Hz).

The incident beam scanning can be modeled by inclusion of a position-dependent parameter $T(u)$, where u is the displacement at the retina of the incident beam from the photoreceptor axis, and in a first approximation by replacing the pinhole in Eq. (2) with $T(u)\mathcal{P}(\mathbf{r})$. This takes into account changes in the photoreceptor-to-light coupling as the focused beam sweeps across each photoreceptor aperture during the raster scan [ideally, $T(u)$ should act on the object before the convolution with the pinhole thereby increasing the complexity of the model]. This approximation is most valid when the beam illuminates several receptors simultaneously. If focused tightly, to a spot size comparable with the photoreceptor spacing, a different modeling would be required as the light may couple to a single photoreceptor at a time. If aberrations of the incident light can be ignored, as may be the case for a narrow beam, a position-dependent coupling efficiency can be estimated as[14]

$$T(u) = \left[\frac{2w_r w_m}{w_r^2 + w_m^2}\right]^2 \exp\left[\frac{-2u^2}{w_r^2 + w_m^2}\right], \quad (3)$$

where w_r is the focused spot size at the retina of an incident Gaussian beam. Equation (3) results from a calculation of the overlap integral between the incident amplitude field and the fundamental mode of the photoreceptor waveguide. Inclusion of this position-dependent parameter can be expected to reduce the blur of each cone in simulated images, although a better estimate should also include the aberrations of the incident beam. It should be mentioned that the retinal object may be extracted from the resulting image by inverting Eq. (2) and removing the influence of measured aberrations. However, because of the low-pass filtering of images by the finite-sized confocal pinhole, noise in the recorded data, and the uncertainty in measurements of Φ_{WA}, this is not easily accomplished.

In summary, to resolve the photoreceptor mosaic requires obviously either a pinhole smaller than the spacing of the imaged receptors, or alternatively that only a single photoreceptor is exposed to light at a time as by a tightly focused (aberration-corrected) incident beam.[4] The influence of $T(u)$ on the recorded image quality may, together with a faster acquisition, plausibly explain why the apparently best high-resolution cone mosaic images to date have been obtained with flood illumination systems,[1,2] since in this case $T(u)$ may be considered approximately constant. In a scanning system, its influence may change the amount of coupled light (and thereby also the signal) each time a given photoreceptor is scanned. In the following, we examine numerically the possibilities of cone mosaic imaging with a tiny pinhole in the c-SLO tailored to directional-light detection.

3. NUMERICAL RESULTS AND COMPARISON WITH EXPERIMENTS

The actual c-SLO has been calibrated by scanning a copper-on-glass mesh of 63.5 μm period through an achromatic lens (25 mm focal length). A conversion factor of 280 μm/degree has been used for the eye, and based on this calibration all of the following images cover 140 $\times$ 140 μm at the retina (with 256$\times$256 pixels). Experimentally obtained results for different pinhole sizes are shown in Fig. 2. To reduce the influence of aberrations on the incident beam its diameter has been restricted to 2.0 mm at the eye pupil. For the near-IR wavelength $\lambda = 0.785$ μm used in the experiments, this corresponds at best to an ≈ 8 μm bright spot on the retina. With a sufficiently small pinhole the presence of the photoreceptor mosaic becomes apparent in the recorded images as reported previously.[7] To simulate the situation, cone photoreceptors have been distributed in a hexagonal arrangement with added random jitter (each one bounded in a hexagonal area to avoid overlapping cones) thereby re-

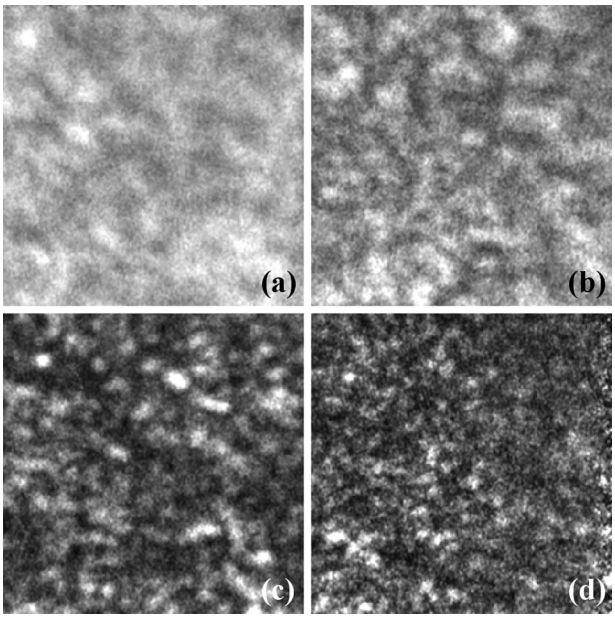

Fig. 2. Experimental images (correlation of 6–8 consecutive frames) obtained with a 0.785 μm wavelength laser diode in the right eye at $\approx 2°$ nasal with different-sized pinholes: (a) 200, (b) 100, (c) 50, (d) 30 μm. In (d) a small signal-to-noise ratio hinders high image quality. Ocular motion prevents repeated recording of exactly the same retinal location and images are therefore somewhat shifted with respect to each other.

sembling the *in vitro* photoreceptor distributions studied by Curcio *et al.*[23]

Figures 3 and 4 show simulated distributions of cones (Gaussian beam intensity images) for densities $\sigma = 10{,}000/\mathrm{mm}^2$ and $20{,}000/\mathrm{mm}^2$, respectively (corresponding to typical cone spacings, $l_c = 1.075/\sigma^{1/2}$, of ≈ 10.75 μm and ≈ 7.60 μm), and simulated c-SLO images for different confocal pinholes. The wavefront aberration used in the calculation is the experimentally recorded one shown in Fig. 1. To match the situation at the periphery of the fovea we have chosen $w_m = 1.50$ μm for the quasi-Gaussian mode (corresponding to an inner segment diameter of approximately 3.6 μm[14]). This mode results in a spot size of $w_p = 2.78$ mm at the pupil for the near-IR wavelength used. A smaller width at the pupil can be obtained with a larger w_m (i.e., for wider cones) or for a shorter wavelength of illumination.

From the results obtained it is apparent that a sufficiently small pinhole (comparable to the photoreceptor spacing when imaged onto the retina) can reveal the underlying photoreceptor mosaic as suggested by Eq. (2) and

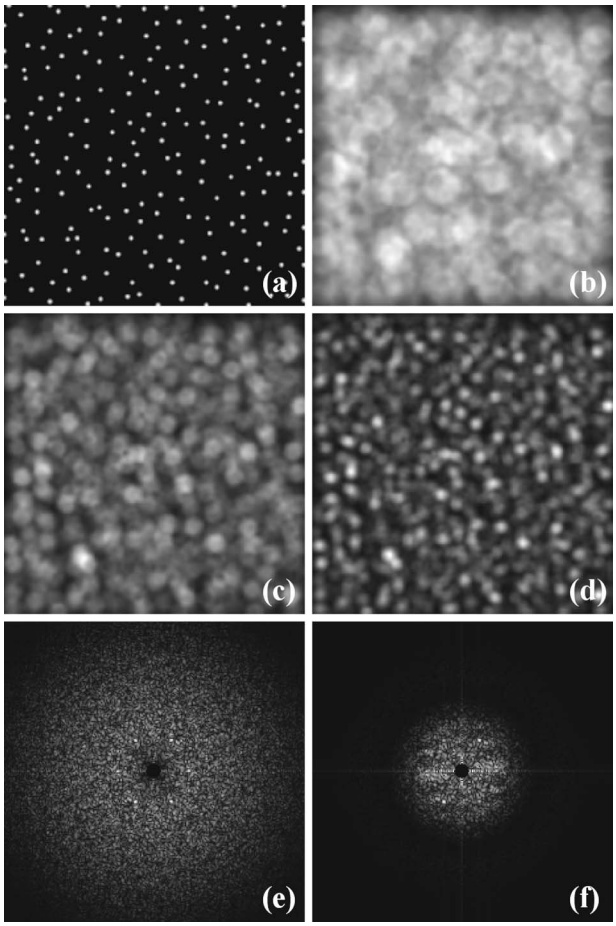

Fig. 3. Simulated (a) retinal section for a cone density of $10{,}000/\mathrm{mm}^2$ and corresponding c-SLO images for pinholes of (b) 100, (c) 50, (d) 30 μm. The imaged retina is 6-times magnified in the plane of the pinhole. Corresponding two-dimensional amplitude spectra of (a) and (d) are shown in (e) and (f), respectively, (to enhance contrast of the hexagonal frequency pattern the central part of each spectrum has been suppressed). The wavefront aberration used in the simulation is the experimentally obtained one shown in Fig. 1(b).

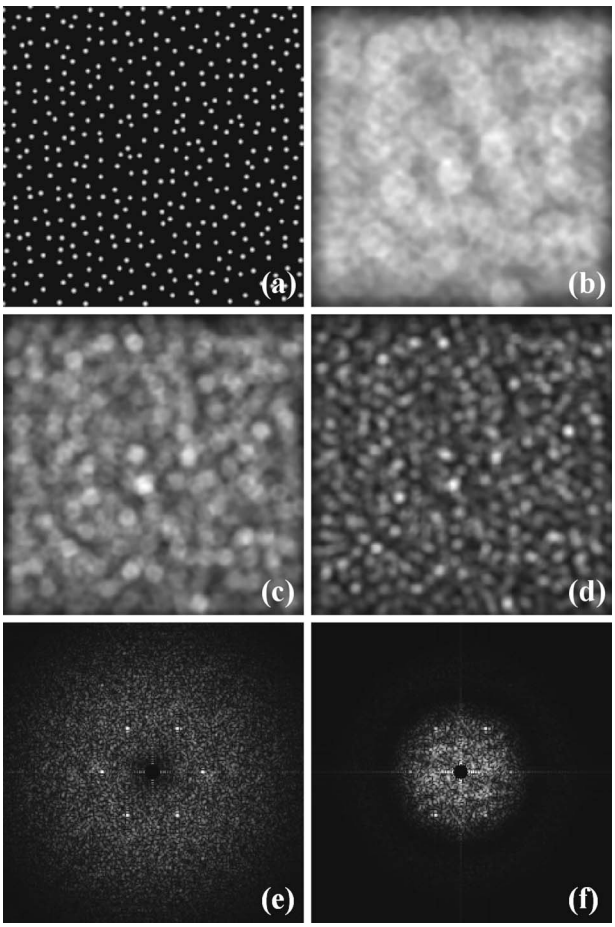

Fig. 4. Simulated (a) retinal section for a cone density of $20{,}000/\mathrm{mm}^2$; otherwise, details are the same as in Fig. 3.

as verified also by the spectral images. The larger pinhole smears out any detailed structure with only some contrast produced by the variation in the number of simultaneously scanned cones (as contained within the area of the pinhole) and by interference among the contributing light beams. In reality, the simulated case of the large pinhole is perchance somewhat exaggerated since the incident beam hardly couples equally well to all contributing photoreceptors, thereby violating the assumption of equal radiation from all (see Fig. 6 below). As the pinhole is reduced the image resembles more closely the structure of the original object, but the relationship is not a simple one because of the overlap of light from neighboring cones and the loss in resolution due to the finite pinhole size. Thus, only in some cases can bright spots be unambiguously identified with the presence of a corresponding photoreceptor. Moreover, the greater the photoreceptor density the harder it becomes to identify contributions from individual receptors.

To examine the image-deteriorating effect of aberrations more closely, the process has been simulated with different scalings of Φ_{WA} producing the results shown in Fig. 5. It can be seen that even with all aberrations corrected, the image differs from the object because of the blurring by the pinhole [cf. Fig. 5(d) and Fig. 3(a)]. The resulting resolution loss prevents the distinction of closely spaced photoreceptors although an increased brightness

(when in phase) indicates the presence of more than one. If the phase of each Gaussian beam is allowed to vary arbitrarily, which may be the case if many photoreceptors contribute at a time with a poorly focused incident beam,[14] the image appearance does not change significantly apart from some redistribution of brightness (for simplicity not shown here).

We have also examined the consequences of including the incident beam scanning in the model by taking a 2.0 mm wide (untruncated) incident beam at the eye pupil

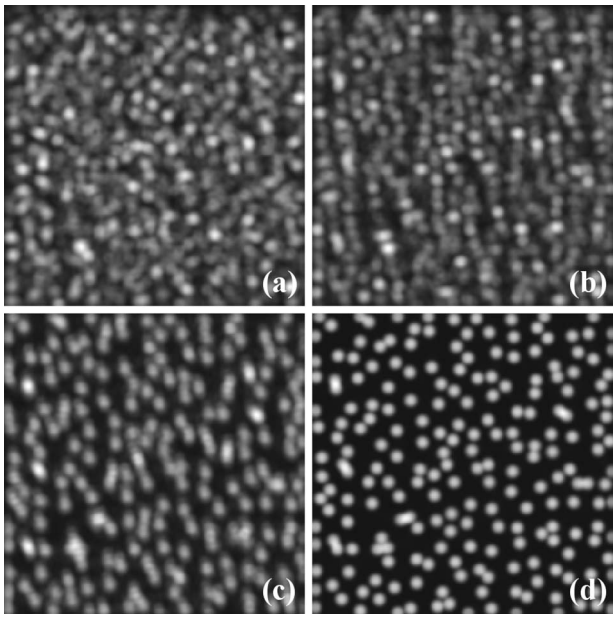

Fig. 5. Simulated c-SLO images for a cone density of 10,000/mm^2 and a 30 μm pinhole for different amounts of the wavefront aberration Φ_{WA} shown in Fig. 1(b): (a) Φ_{WA} same as in Fig. 3(d), (b) $\Phi_{WA}/2$, (c) $\Phi_{WA}/4$, (d) no aberrations (corresponding to a completely corrected wavefront).

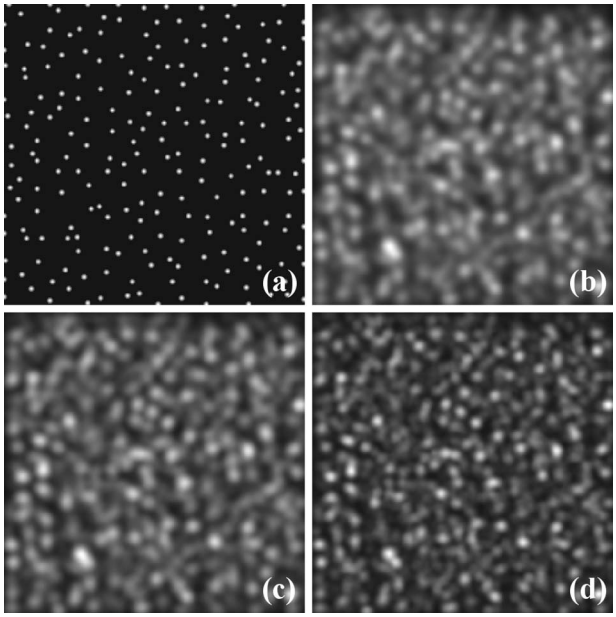

Fig. 6. Same as Fig. 3 but with the inclusion of incident beam scanning. For simplicity the spectral images are not shown.

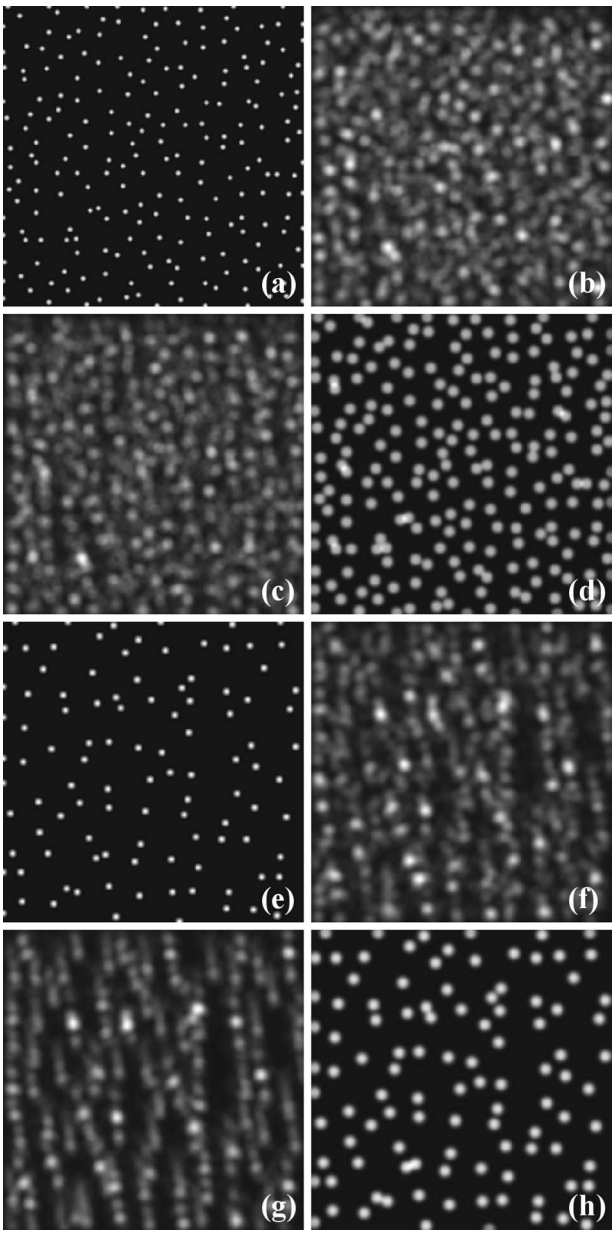

Fig. 7. Simulated c-SLO images (b), (c), (d) and (f), (g), (h) with 30 μm pinhole for objects (a) 10,000/mm^2 with $w_m = 1.50$ μm, (e) 5000/mm^2 with $w_m = 2.00$ μm, respectively. Images of the objects are shown at wavelengths of (b), (f) 0.785 μm; (c), (g) 0.543 μm, all with the aberration map shown in Fig. 3(b); (d), (h) 0.543 μm without aberrations. Note that (a) and (b) are identical to Fig. 3(a) and Fig. 3(d), respectively, but have been reproduced here for ease of comparison.

(corresponding to $w_r \approx 4.2$ μm), and letting it act as a Gaussian weighting of the pinhole in accordance with Eq. (3). The results obtained (Fig. 6) show a sharpening of details, but perhaps most apparent when compared to Fig. 3 is the absence of circular structures (pinhole images) when larger pinholes are used. Thus, the situation comes closer to the experimentally realized one, although proper inclusion of the incident beam aberrations in $T(u)$ is expected to produce an even greater resemblance.

Finally, the influence of the chosen illumination wavelength has been considered. Near-IR has some clear advantages over the visible in the context of imaging apart

from the comfort of the subject: More light can be used without compromising safety, and a larger fraction of light will travel the full photoreceptor length as a result of low absorption in the outer segment thereby not requiring prebleaching. However, the width of the directional light at the pupil scales with the wavelength squared[24] and is therefore more prone to suffer aberrations at longer wavelengths. Moreover, the overall amount of reflected (nondirectional) light increases with wavelength[25,26] making the omission of a uniform background at the pupil more problematic in the present model. The outcome of simulations at two different illumination wavelengths is shown in Fig. 7 (again leaving out the incident beam scanning). For comparison also a low-density photoreceptor section has been simulated (with slightly wider cones). The image quality is slightly better at the lower wavelength because of the smaller influence of aberrations as discussed above. However, the improvement is not dramatic and again the imaged cones cannot be clearly distinguished unless their local density is low or, alternatively, wavefront correction is used together with a tiny pinhole.

4. CONCLUSIONS

In this paper, our recently proposed directional light c-SLO[7] has been examined in further detail with numerical simulations of cone-mosaic images obtained under different conditions. Since the photoreceptors are known to be wave-guiding structures, the description is formulated by considering each photoreceptor to radiate independently a Gaussian beam (resembling the fundamental mode of the inner segment) when exposed to light. We found that the results agree qualitatively well with observations made in the real eye confirming that although a small pinhole can reveal the photoreceptor mosaic off the fovea it requires wavefront correction to be reliably resolved when the density is large. For simplicity of modeling the focused beam on the retina has been assumed wider than the intercone distance, thereby exposing several photoreceptors at a time. In experiments, the situation can be expected to improve since the small width of the incident beam, together with any fine structure in the focus, may act as a resolution-enhancing filter by favoring the coupling of light to a single photoreceptor at a time and thereby highlighting its contribution. Although such a situation is not controllable for accurate photoreceptor mosaic imaging, it may suffice to reveal areas of misoriented photoreceptors[27] as well as other retinal abnormalities.

ACKNOWLEDGMENTS

The authors gratefully acknowledge financial support from the Ministerio de Educación y Ciencia (grant BFM2001-0391 and FIS2004-02153), Spanish Fondo de Investigación Sanitaria (grant red IM3 G03/185), and Ramón y Cajal research contract RYC2002-006337.

Corresponding author Brian Vohnsen's e-mail address is vohnsen@um.es.

REFERENCES

1. J. Liang, D. R. Williams, and D. T. Miller, "Supernormal vision and high-resolution retinal imaging through adaptive optics," J. Opt. Soc. Am. A **14**, 2884–2892 (1997).
2. A. Roorda and D. R. Williams, "The arrangement of the three cone classes in the living human eye," Nature (London) **397**, 520–522 (1999).
3. E. J. Fernández, I. Iglesias, and P. Artal, "Closed-loop adaptive optics in the human eye," Opt. Lett. **26**, 746–748 (2001).
4. A. Roorda, F. Romero-Borja, W. J. Donnelly III, H. Queener, T. J. Hebert, and M. C. W. Campbell, "Adaptive optics scanning laser ophthalmoscopy," Opt. Express **10**, 405–412 (2002).
5. A. R. Wade and F. W. Fitzke, "*In vivo* imaging of the human cone-photoreceptor mosaic using a confocal laser scanning ophthalmoscope," Lasers Light 8, 129–136 (1998).
6. A. R. Wade and F. W. Fitzke, "A fast, robust pattern recognition system for low light level image registration and its application to retinal imaging," Opt. Express **3**, 190–197 (1998).
7. B. Vohnsen, I. Iglesias, and P. Artal, "Directional imaging of the retinal cone mosaic," Opt. Lett. **29**, 968–970 (2004).
8. W. S. Stiles and B. H. Crawford, "The luminous efficiency of rays entering the eye pupil at different points," Proc. R. Soc., London, Ser. B **112**, 428–450 (1933).
9. A. W. Snyder and C. Pask, "The Stiles–Crawford effect-explanation and consequences," Vision Res. **13**, 1115–1137 (1973).
10. P. J. Delint, T. T. J. M. Berendschot, and D. van Norren, "Local photoreceptor alignment measured with a scanning laser ophthalmoscope," Vision Res. **37**, 243–248 (1996).
11. S. A. Burns, S. Wu, F. Delori, and A. E. Elsner, "Direct measurement of human-cone-photoreceptor alignment," J. Opt. Soc. Am. A **12**, 2329–2338 (1995).
12. S. A. Burns, S. Wu, J. C. He, and A. E. Elsner, "Variations in photoreceptor directionality across the central retina," J. Opt. Soc. Am. A **14**, 2033–2040 (1997).
13. J. C. He, S. Marcos, and S. A. Burns, "Comparison of cone directionality determined by psychophysical and reflectometric techniques," J. Opt. Soc. Am. A **16**, 2363–2369 (1999).
14. B. Vohnsen, I. Iglesias, and P. Artal, "Guided light and diffraction model of human-eye photoreceptors," J. Opt. Soc. Am. A **22**, 2318–2328 (2005).
15. A. Pallikaris, D. R. Williams, and H. Hofer, "The reflectance of single cones in the living human eye," Invest. Ophthalmol. Visual Sci. **44**, 4580–4592 (2003).
16. J.-M. Gorrand and F. C. Delori, "A model for assessment of cone directionality," J. Mod. Opt. **44**, 473–491 (1997).
17. A. M. Laties and J. M. Enoch, "An analysis of retinal receptor orientation," Invest. Ophthalmol. Visual Sci. **10**, 69–77 (1971).
18. R. H. Webb, G. W. Hughes, and F. C. Delori, "Confocal scanning laser ophthalmoscope," Appl. Opt. **26**, 1492–1499 (1987).
19. S. A. Burns, S. Marcos, A. E. Elsner, and S. Bara, "Contrast improvement of confocal retinal imaging by use of phase-correcting plates," Opt. Lett. **27**, 400–402 (2002).
20. B. Vohnsen, I. Iglesias, and P. Artal, "Confocal scanning laser ophthalmoscope with adaptive optical wavefront correction," in Proc. SPIE **4964**, 24–32 (2003).
21. P. M. Prieto, F. Vargas-Martín, S. Goelz, and P. Artal, "Analysis of the performance of the Hartmann–Shack sensor in the human eye," J. Opt. Soc. Am. A **17**, 1388–1398 (2000).
22. S. Marcos, S. A. Burns, and J. C. He, "Model for cone directionality reflectometric measurements based on scattering," J. Opt. Soc. Am. A **15**, 2012–2022 (1998).
23. C. A. Curcio, K. R. Sloan, R. E. Kalina, and A. E. Hendrickson, "Human photoreceptor topography," J. Comp. Neurol. **292**, 497–523 (1990).
24. N. P. A. Zagers, T. T. J. M. Berendschot, and D. van Norren, "Wavelength dependence of reflectometric cone

photoreceptor directionality," J. Opt. Soc. Am. A **20**, 18–23 (2003).
25. N. P. A. Zagers, J. van de Kraats, T. T. J. M. Berendschot, and D. van Norren, "Simultaneous measurement of foveal spectral reflectance and cone-photoreceptor directionality," Appl. Opt. **41**, 4686–4696 (2002).
26. J. J. Vos, A. A. Munnik, and J. Boogaard, "Absolute spectral reflectance of fundus oculi," J. Opt. Soc. Am. **55**, 573–574 (1965).
27. M. Kono, J. M. Enoch, E. Strada, P. Shih, R. Srinivasan, V. Lakshminarayanan, W. Susilasate, and A. Graham, "Stiles–Crawford effect of the first kind: assessment of photoreceptor alignments following dark patching," Vision Res. **41**, 103–118 (2001).